Metal-free g-C$_3$N$_4$ photocatalyst by sulfuric acid activation for selective aerobic oxidation of benzyl alcohol under visible light

Ligang Zhang [a,b], Di Liu [a,c], Jing Guan [a], Xiufang Chen [a,*], Xingcui Guo [a], Fuhua Zhao [a,b], Tonggang Hou [a], Xindong Mu [a,*]

[a] Key Laboratory of Biobased Materials, Qingdao Institute of Bioenergy and Bioprocess Technology, Chinese Academy of Sciences, Qingdao 266101, PR China
[b] University of Chinese Academy of Sciences, Beijing 100049, PR China
[c] Ocean University of China, Qingdao 266003, PR China

A B S T R A C T

In this work, modification of graphitic carbon nitride photocatalyst with acid was accomplished with a facile method through reflux in different acidic substances. The g-C$_3$N$_4$-based material was found to be a metal-free photocatalyst useful for the selective oxidation of benzyl alcohol with dioxygen as the oxidant under visible light irradiation. Acid modification had a significant influence on the photocatalytic performance of g-C$_3$N$_4$. Among all acid tested, sulfuric acid-modified g-C$_3$N$_4$ showed the highest catalytic activity and gave benzaldehyde in 23% yield for 4 h under visible light irradiation, which was about 2.5 times higher than that of g-C$_3$N$_4$. The acid modification effectively improved surface area, reduced structural size, enlarged band gap, enhanced surface chemical state, and facilitated photoinduced charge separation, contributing to the enhanced photocatalytic activity. It is hoped that our work can open promising prospects for the utilization of metal free g-C$_3$N$_4$-based semiconductor as visible-light photocatalyst for selective organic transformation.

1. Introduction

The selective oxidation of alcohols into corresponding aldehydes or ketones is one of the most-fundamental reactions in organic synthesis and chemical industry [1]. Traditionally, toxic, environmentally harmful oxidants and harsh conditions such as toxic metal oxides [2,3], peroxides [4,5], high temperature and pressure were required for these transformations. Compared with the conventional chemical methods, the use of solar radiant energy to drive organic reactions provides a sustainable pathway for green synthesis [6–8]. However, the strong oxidative potential of radicals and holes formed on the surface of photocatalysts in the UV-induced chemical reactions always promote a complete mineralization, leading to photocatalysis unselective. To bypass these drawbacks, organic transformations by visible-light photocatalysis are favored in order to facilitate higher selectivity. Nevertheless, there exists very few visible-light photocatalysts suitable for selective organic transformations [9,10]. Therefore, one of the challenges is to explore novel and efficient visible-light photocatalysts for the selective organic transformations.

In recent years, much effort has been devoted to the development of visible-light-driven photocatalysts for selective oxidation of alcohols to carbonyl compounds. For example, Bi$_2$WO$_6$ were demonstrated to catalyze the aerobic oxidation of alcohols [11,12]. Several TiO$_2$-based [13–18] and CdS-based [15,19–22] catalysts showed photoactivity for aerobic oxidation of alcohols to corresponding aldehydes. However, most of the reported photocatalysts used for selective oxidation of alcohols are focused on metal-based inorganic semiconductors, such as metal oxide [13,14], metal sulfides [23] or metal nitrides [24]. The design, preparation and modification of earth-abundant elemental photocatalysts that are efficient and adequately stable are still in its infancy.

During the search for earth-abundant elements to construct efficient visible-light-driven photocatalysts, polymeric g-C$_3$N$_4$ has attracted a great deal of interest in photocatalytic applications [25–28]. Compared with metal-based catalysts, g-C$_3$N$_4$ has advantages of low cost, good chemical stability, no heavy metal pollution and environmental friendliness. More interestingly, the g-C$_3$N$_4$ material has attractive electronic structure with a visible-light driven band gap of 2.7 eV. The bottom of the conduction band of g-C$_3$N$_4$ is −1.3 V, which is high enough to activate molecular oxygen for selective oxygenation of organic substrates. Meanwhile, the top of the valence band is 1.4 V, which is too low to directly oxidize water

* Corresponding author. Tel.: +86 532 8066 2725; fax: +86 532 8066 2724.
 *E-mail addresses:* muxd@qibebt.ac.cn, greencc@qibebt.ac.cn (X. Mu).
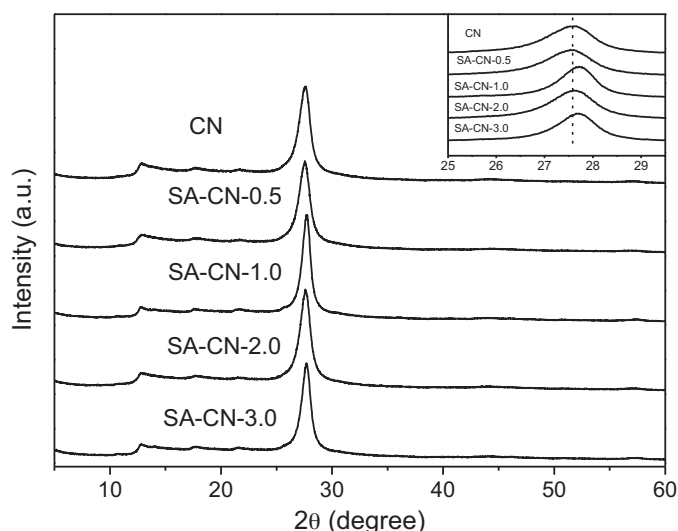
Fig. 1. XRD patterns of CN and SA-CN samples with different molarities solutions of sulfuric acid. The inset shows the region of the main peak at 27.6°.

or hydroxyl group to form a free hydroxyl radical in thermodynamics. Moreover, g-C$_3$N$_4$ can be easily prepared by the condensation of the cheap raw materials like dicyandiamide, melamine, triazine, heptazine derivatives, thiourea and urea [29]. In addition, the structure of g-C$_3$N$_4$ is flexible, which allows plentiful organic schemes to tailor its chemical structure for the improvement of its catalytic activity [30]. These unique properties, along with its low price, make g-C$_3$N$_4$ a promising candidate for applications in solar photocatalysis for selective organic transformations. Nevertheless, most research works are focused on utilizing g-C$_3$N$_4$-based photocatalysts in the fields of water splitting [9,28,31,32] and the elimination of organic pollutants [33,34]. g-C$_3$N$_4$-based semiconductors was also demonstrated to serve as metal-free photocatalysts to catalyze the selective organic synthesis, such as alcohol oxidation, alkane oxidation and olefins oxidation [25,27]. However, bulk g-C$_3$N$_4$ suffers from major drawbacks such as rapid recombination of photogenerated electron-hole carriers, low solar utilization efficiency and low BET surface area ($\sim$10 m^2 g^{-1}). Mesoporous carbon nitride materials used by Wang et al. was prepared by hard-templating method, which required strong acid (NH$_4$HF$_2$ or HF) treatment to
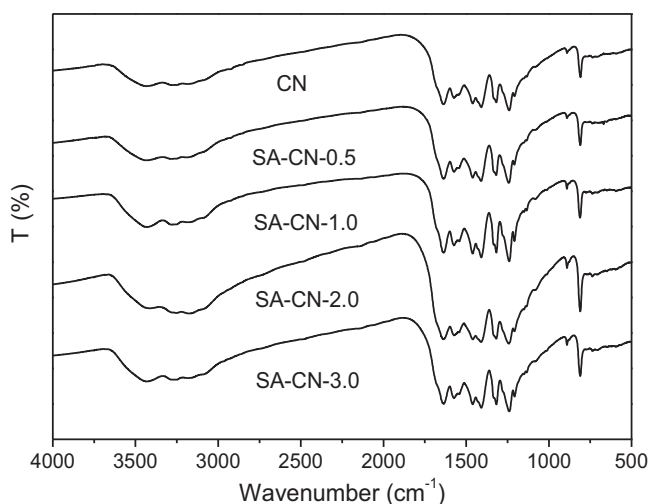
Fig. 2. FTIR spectra of bulk g-C$_3$N$_4$ and SA-CN samples with different molarities solutions of sulfuric acid.
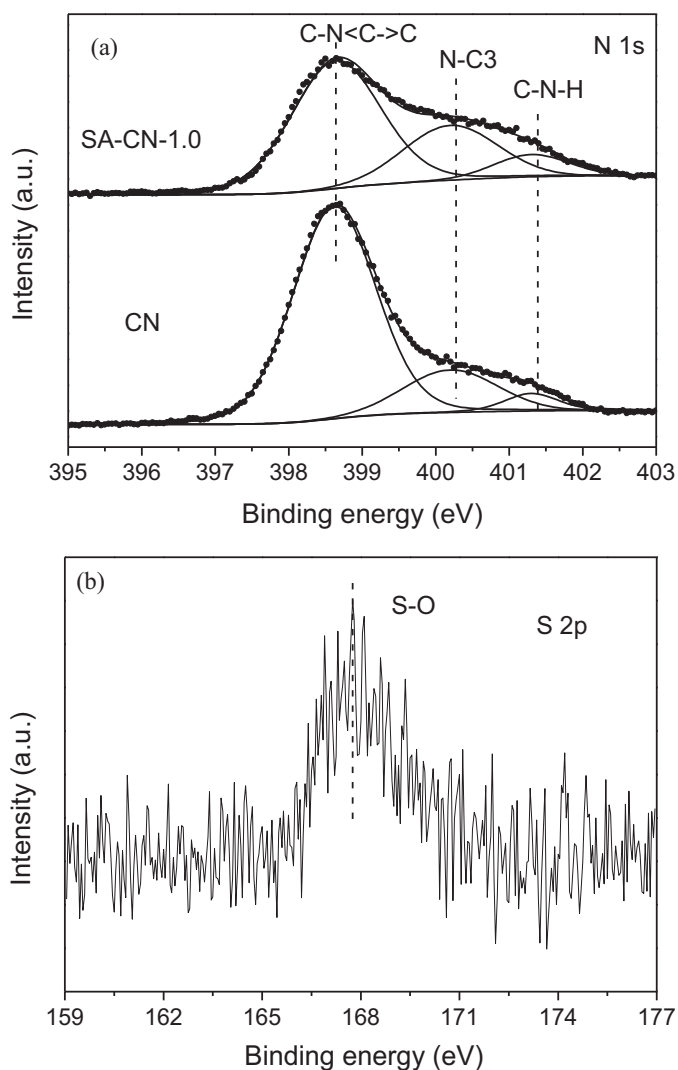
Fig. 3. XPS spectra of N 1s (a) of CN and SA-CN-1.0 sample and S 2p (b) of SA-CN-1.0 sample.

remove silica templates [25]. Harmful, toxic and multi-step procedures are problems to restrict its practical application. Therefore, it is essential to explore reliable and facile strategies to fabricate the active g-C$_3$N$_4$-based photocatalysts for selective organic synthesis.

Activation of base functionalities with acid is a convenient modification route to tune the electronic structure, which modified the surface structure of carbon nitride materials with enhanced ionic conductivity [35,36]. For other polymer semiconductors, polyamidoamine dendrimers were activated by acid to enhance proton conductivity [37]. It has been reported that in photoredox catalytic reactions, mineral acid was used with promotion effect on the alcohol oxidation process [38], however, the subsequent isolation of the homogeneous acid is still a difficult reaction step. The acid-promoted photosynthesis encouraged us to activate carbon nitride by direct protonation with Brønsted acid. The acid activation of carbon nitride would result in the formation of new Brønsted acid sites on its surface. It is believed that the catalytic performance of the g-C$_3$N$_4$-based photosystem could be tuned by coupling with acid catalysis. From the standpoint of green and sustainable chemistry, the application of acid-modified g-C$_3$N$_4$ photocatalysts in selective organic transformations is highly desirable but remains unexplored.

Table 1
Result of curve-fitting of the high-resolution XPS spectra for the N 1s region.

Catalyst	N 1s (%)	N 1s (C—NC) (%)	N 1s N—C$_3$ (%)	N 1s C—N—H (%)
CN	59.1	46.5	9.9	2.7
SA-CN-1.0	57.0	36.6	15.4	5.0

In our work, the modification of g-C$_3$N$_4$ with acid was used to tune the photocatalytic performance of carbon nitride photocatalysts. The acid-modified carbon nitride was prepared with a facile method through reflux in a series of acid solutions, including sulfuric acid, nitric acid, hydrochloric acid, phosphoric acid, formic acid, acetic acid, benzenesulfonic acid and perchloric acid. The acid modification of the carbon nitride was systematically investigated by adjusting a series of activation conditions at various acid/carbon nitride mass ratios and activation time. The effects of acid activation on textural, electronic, optical, and surface properties, as well as photocatalytic activity of g-C$_3$N$_4$ were also investigated. The photocatalytic activity of the synthesized g-C$_3$N$_4$-based catalysts was evaluated by selective oxidation of benzyl alcohol with O$_2$ and visible light at atmospheric pressure.

2. Experimental

2.1. Catalyst preparation

Bulk g-C$_3$N$_4$: 2.5 g of dicyandiamide was heated to 550 °C for 5 h in a muffle furnace in air. The sample was then cooled to room temperature.

Acid modified g-C$_3$N$_4$: 1 g of as-prepared bulk g-C$_3$N$_4$ solid was ground well and then put into 100 mL sulfuric acid (0.5–3 M) and refluxed at 135 °C for the required time (6–48 h). The solid product was then collected by centrifugation and washed with deionized water for several times. Then, the product was dried at 60 °C in a vacuum oven. For comparison, g-C$_3$N$_4$ solid was also treated by 1 M other acids (nitric acid, hydrochloric acid, phosphoric acid, formic

acid, acetic acid, benzenesulfonic acid and perchloric acid) for 24 h by the similar procedure. The bulk g-C$_3$N$_4$ sample is denoted as CN. The sample by the activation of sulfuric acid is denoted as SA-CN-n, where the number of n stands for the concentration of sulfuric acid. For example, SA-CN-1.0 means g-C$_3$N$_4$ samples treated with 1 M sulfuric acid. The sample by the treatment of nitric acid, hydrochloric acid, phosphoric acid, formic acid, acetic acid, benzenesulfonic acid or perchloric acid was denoted as NA–CN, HA–CN, PhA–CN, FA–CN, AA–CN, BA–CN or PeA–CN, respectively.

2.2. Characterization

The phase composition of the samples was analyzed on a Bruker D8 Advance X-ray diffraction (XRD) diffractometer with CuKa radiation (λ = 1.5147 Å). A Thermo Nicolet FTIR Spectrometer was used to obtain the Fourier transformed infrared (FTIR) spectra. A vario EL cube from Elementar Analysensysteme GmbH was employed to conduct elemental analysis. The morphology of catalysts was determined by means of a field emission-TEM (H-7600) and SEM (Hitachi S-4800) microscope. Nitrogen sorption experiments were carried out at 77 K using a micromeritics ASAP 2020 m + c sorptometer. The samples were degassed in a vacuum at 150 °C for 6 h prior to measurement. X-ray photoelectron spectra (XPS) data were recorded on a Thermo ESCALAB250 instrument with a monochromatized Al Kα line source. All the binding energies were referenced to the C 1s peak at 284.6 eV. The light absorption spectra were obtained using a HITACHI U-4000 Spectrophotometer equipped with a Labsphere diffuse reflectance accessory. Photoluminescence (PL) spectra were measured at 298 K on the Fluoro-max-4 spectrofluorometer.

2.3. Photocatalytic activity

The photocatalytic activity of g-C$_3$N$_4$-based catalysts was investigated by the selective oxidation of benzyl alcohol with
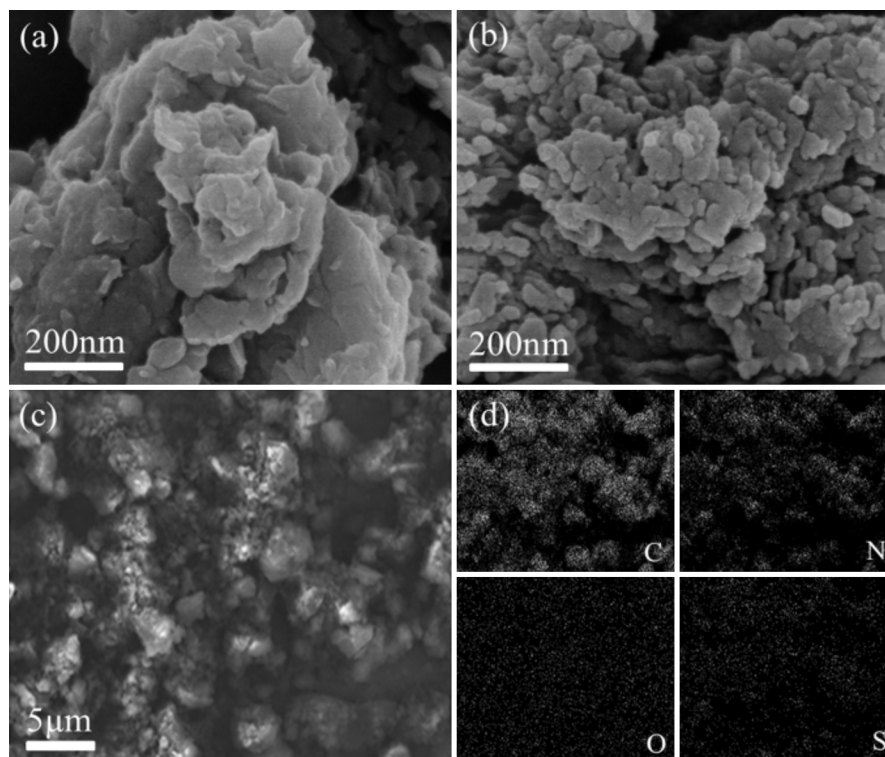
Fig. 4. Typical SEM images of bulk g-C$_3$N$_4$ (a), SA-CN-1.0 (b) and its images (c) and the corresponding elemental mapping images of C, N, O and S (d).
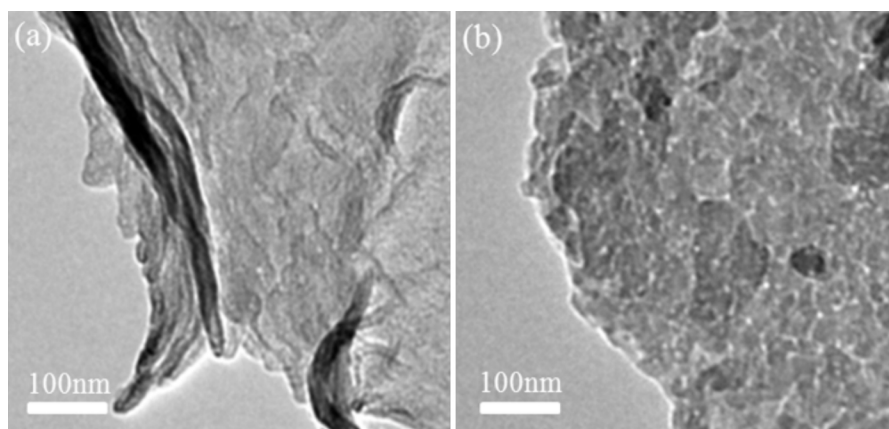
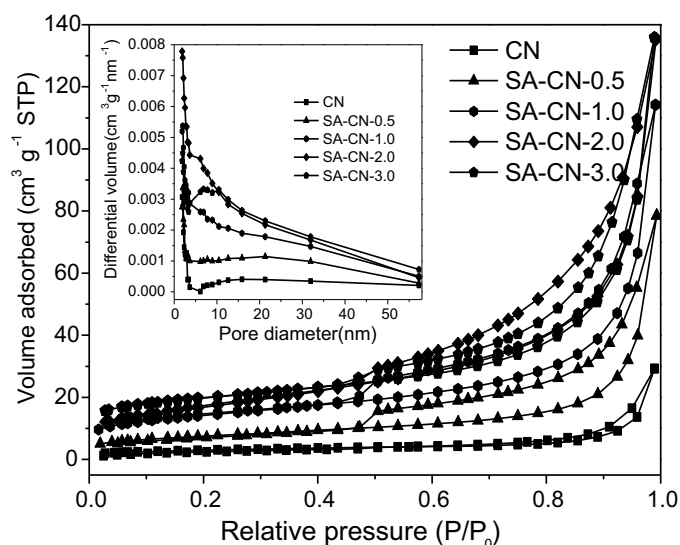**Fig. 5.** Typical TEM images of bulk g-C$_3$N$_4$ (a) and SA-CN-1.0 (b) sample.

Fig. 6. N$_2$ adsorption–desorption isotherm and the pore size distribution (inset) of bulk g-C$_3$N$_4$ and SA-CN catalysts with different molarities solutions of sulfuric acid.

molecular O$_2$ as oxidant under visible light irradiation. In a typical reaction, photocatalytic activity measurements were carried out in a 25 mL glass reaction flask fitted with a condenser and a magnetic stirrer. The visible-light source for the reaction was provided by a 300 W Xenon lamp with a 420 nm cut-off filter. Benzyl alcohol (1 mmol), the catalyst (50 mg) and trifluorotoluene (10 mL) were added to the flask reactor. O$_2$ (pressure ca. 1 bar) collected in a rubber bag was connected to the system. The resulting system was then stirred at 100 °C for 4 h under visible light irradiation. After the reaction, the solid catalyst was separated by centrifugation. The liquid phase was analyzed by a gas chromatograph (VARIAN 450)

with anisole as the internal standard. In addition, different radical scavengers were used in the controlled photoactivity experiments, which involved -butyl alcohol (TBA, as trapping agent for hydroxyl radical species), benzoquinone (BQ, as trapping agent for superoxide radical species) and ammonium oxalate (AO, as trapping agent for holes). The amount of the above scavengers was 1 mmol.

3. Results and discussion

3.1. Characterization of acid-modified g-C$_3$N$_4$

The structures of CN and SA-CN samples treated with different concentrations of sulfuric acid were studied by XRD. As shown in Fig. 1, all of the CN and SA-CN samples display two characteristic XRD peaks, which were commonly found in carbon nitride. The intense peak focused on 27.6° is the typical graphite interlayer [39], which is marked as 0 0 2 peak and the interplanar distance was $d = 0.33$ nm. The other peak at 12.8° (index as 100, $d = 0.69$ nm) shows a two dimensional packing motif. The XRD results demonstrated that the typical graphite-like structure of CN-based materials is still maintained after sulfuric acid treatment. For SA-CN samples, when the sulfuric acid concentration is higher than 1 M, the (0 0 2) peak is shifted slightly to higher angle whereas the (1 0 0) peak remains unchanged at 12.8°, reflecting a slight decrease of the interlayer spacing ($d_{0 0 2}$) and a structural compaction by the treatment of sulfuric acid [40,41].

The change in the chemical composition of g-C$_3$N$_4$ caused by sulfuric acid treatment was analyzed by elemental analysis (Table S1). It was found that both the average C/N ratio value and hydrogen content were slightly increased after sulfuric acid treatment. The average C/N ratio value increased from 0.66 for CN to 0.67 for SA-CN. Correspondingly, the hydrogen contents increased from 1.7% for CN to 1.9% for SA-CN. The increased

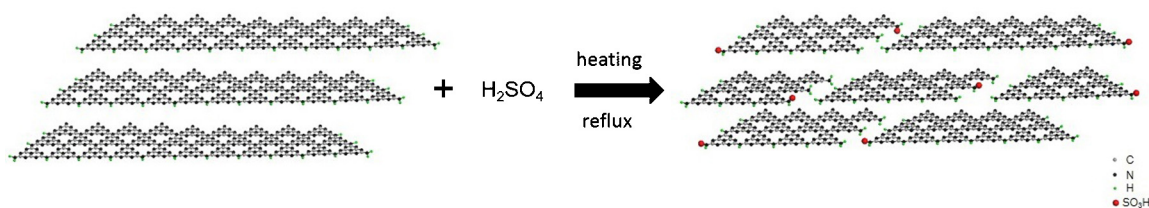**Fig. 7.** A schematic illustration of synthesis of SA-CN catalysts (the gray, black, green and red balls represent C, N, H and SO$_3$H, respectively). (For interpretation of the references to colour in this figure legend, the reader is referred to the web version of this article).
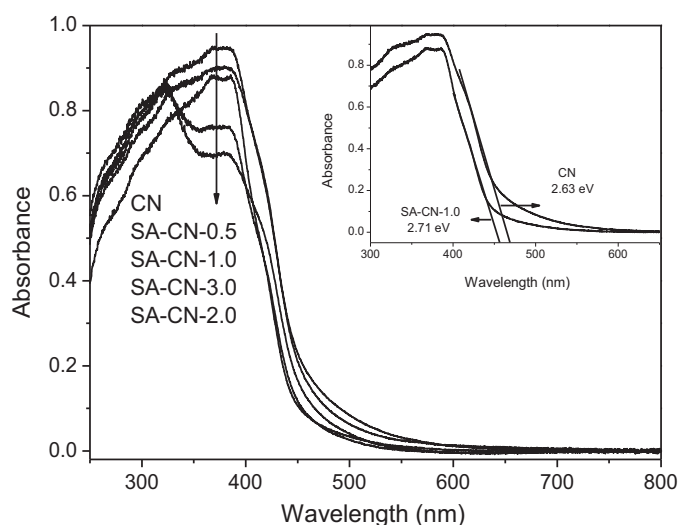
Fig. 8. UV–vis spectra of bulk g-C_3N_4 and SA-CN samples with different molarities solutions of sulfuric acid.

hydrogen content of acid-modified g-C_3N_4 gave direct evidence of the protonation of carbon nitride by acid treatment [35]. It is noteworthy to mention that there is a low content of S in the SA-CN samples (1.3–1.7%), indicating that sulfur-containing groups are linked on the CN surfaces.

The chemical structure of CN and SA-CN samples was investigated by the FTIR spectra, as shown in Fig. 2. All of the samples showed a broad band at around 3000 cm^{-1}, corresponding to amines and incomplete graphitic condensation [42–44]. For the SA-CN samples, the bands in the region of ca. 1100–1600 cm^{-1} and at 800 cm^{-1} were also observed; the former is attributed to C—N heterocyclic stretches, whereas the latter is due to the breathing mode of the tri-s-triazine units, which are also similar to the results of CN. XRD and FTIR results were in good agreement and confirmed that the main structure of g-C_3N_4 is retained after acid treatment. However, there is no obvious N—S [43] or C—S [45] stretch detected in the FTIR spectra, as its vibration might be overlapped by C—N stretches.

The surface chemical compositions and electronic states of the SA-CN sample were further examined by XPS. Fig. 3a shows high-resolution XPS spectra of N 1s of CN and SA-CN-1.0. The N 1s peak can be fitted by three peaks at 398.7, 400.2, 401.3 eV, which are C—NC groups, N—C_3 groups and amino functions carrying
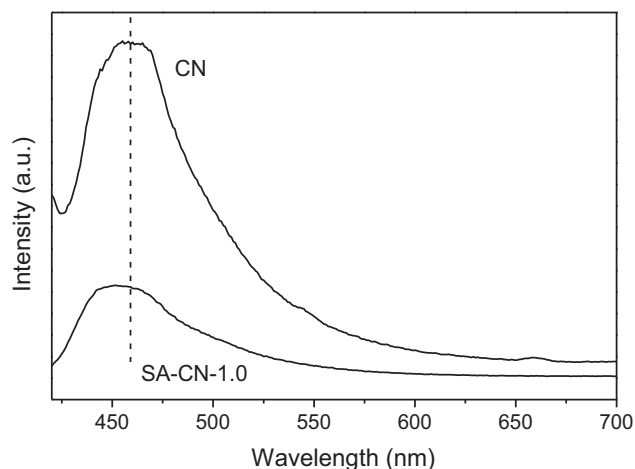

Fig. 9. PL spectra of bulk g-C_3N_4 and SA-CN-1.0 sample at 400 nm excitation at 298 K.

hydrogen (C—N—H) related to structural defects [46], respectively. The detailed results of curve-fitting of the high-resolution XPS spectra for the N 1s region are summarized in Table 1. It is clear that SA-CN-1.0 sample has higher C—N—H content than the pure g-C_3N_4. The higher N content in C—N—H might be originated to amino functions broken up from its defects by acid treatment, which resulted in more defects and acid functionality. The XPS spectra (Fig. 3b) in S 2p region exhibits a broad single peak at around 167.8 eV for SA-CN sample, which is attributable to sulfur in —SO_3H [47]. The calculated surface atomic ratio of O/S content for SA-CN-1.0 was found to be ca. 3.4 at%. This result together with the elemental mapping images (shown in Fig. 4) confirmed that the S atoms in the acid-modified sample are contained in —SO_3H group and —SO_3H group is homogenously distributed in the whole host of acid-modified g-C_3N_4 solid. It should be noted that the acid-modified materials were washed with distilled water repeatedly until sulfate ions were no longer detected in the wash water during the preparation process. The presence of —SO_3H group is attributed to the sulfonation of amino functions (C—N—H) on the surface of carbon nitride. The results illustrate that the acid activation of carbon nitride would result in the formation of new acid sites on its surface.

The morphology of SA-CN was studied by SEM and TEM. As shown in Fig. 4, bulk g-C_3N_4 sample exhibits an aggregated morphology and large particles with a size of several micrometers. SA-CN-1.0 (Fig. 4b) displays a breaking up of both blocks and stacks, turning into many smaller particles after acid treatment. Fig. 5 shows typical TEM images of CN (5a) and SA-CN-1.0 (5b). A two-dimensional structure with small flat sheets stacked and irregular shape were observed in the TEM images of SA-CN-1.0, also quite different from broad stretches and integrated together in CN. Clearly, due to its partly imperfect polymer-like structure, the SA-CN sample is fragmented by acid treatment while the characteristic interplanar stacking structure retains.

The results of nitrogen sorption, summarized in Table S2, showed that the sulfuric acid treatment improved the specific surface area and pore volume of carbon nitride. The specific surface area of g-C_3N_4 was only 10 m^2 g^{-1}, which was much smaller than that of common photocatalysts or catalyst supports. By sulfuric acid treatment, the surface area was significantly increased from 10 m^2 g^{-1} for CN to 66 m^2 g^{-1} for SA-CN-3.0. Correspondingly, the pore volumes also increased from 0.04 cm^3 g^{-1} for CN to 0.21 cm^3 g^{-1} for SA-CN-3.0. The pore-size distribution curves (Fig. 6 inset) showed that a porous structure (2–50 nm) was formed by the acid treatment, which was possibly formed by random-stacking of the fragments. These data illustrated that sulfuric acid treatment could introduce porous structure with increased surface area and enlarged pore volume. Taking into account the results of characterizations, a schematic route of synthesis of SA-CN material is proposed (Fig. 7). It is known that the as-obtained C_3N_4 possessed imperfect polymer-like structure, which contained carbon nitride domains with differential stabilities. When it was treated by sulfuric acid, the unstable domains were preferentially decomposed by sulfuric acid activation to form fragments of relatively stable domains. Meanwhile, it also forms new acid sites (e.g., —SO_3H group) and more structural defects and active sites via acid activation.

Fig. 8 shows the light absorption spectra of CN and SA-CN samples treated with different concentrations of sulfuric acid. It can be seen that the wavelength at the absorption edge of pure g-C_3N_4 was about 471 nm, and the band gap energy was determined to be 2.63 eV. When carbon nitride was treated by sulfuric acid, the light absorption edge of SA-CN showed obvious blue shift, giving rise to an increase in band gap from 2.63 eV of g-C_3N_4 to 2.71 eV of SA-CN-1.0. The blue shift in the band gap reflects the smaller

Table 2
Photocatalytic performances of g-C$_3$N$_4$-based catalysts for oxidation of benzyl alcohol under visible light ($\lambda > 420$ nm).

Entry	Catalysts	hv	Conversion (%)	Benzaldehyde selectivity (%)
1	g-C$_3$N$_4$	–	<1	>99
2	–	+	3.2	>99
3	g-C$_3$N$_4$	+	6.6	>99
4	SA-CN-0.5	+	10.7	>99
5	SA-CN-1.0	+	23.4	98
6	SA-CN-2.0	+	15.3	>99
7	SA-CN-3.0	+	18.8	>99
8	SA-CN-1.0–6 h	+	8.9	>99
9	SA-CN-1.0–12 h	+	10.1	>99
10	SA-CN-1.0–18 h	+	11.5	>99
11	SA-CN-1.0–24 h	+	23.4	98
12	SA-CN-1.0–36 h	+	17.3	>99
13	SA-CN-1.0–48 h	+	14.2	>99

Reaction performed at 100 °C for 4 h using trifluorotoluene as the solvent, 1 mmol benzyl alcohol, 50 mg catalyst. Entries 1–3: the controlled experiments; entries 4–7: bulk g-C$_3$N$_4$ activated by different concentration (0.5–3 M) of sulfuric acid for 24 h; entries 8–13: bulk g-C$_3$N$_4$ activated by 1 M sulfuric acid in different reflux time (6–48 h).

structural size of SA-CN, demonstrating that the unstable domains of g-C$_3$N$_4$ are decomposed by sulfuric acid treatment [29].

More detailed information regarding electronic properties of SA-CN is studied by PL experiments. The PL spectra of CN and SA-CN-1.0 sample under 400 nm are presented in Fig. 9. For pure g-C$_3$N$_4$, one main emission peak appears at about 459 nm. After sulfuric acid treatment, the emission peak shows a blue-shift from 459 to 452 nm, which is in good agreement with the UV–vis spectra. The enlarged band gap is attributed to the well-known quantum confinement effect [48]. Compared to pure g-C$_3$N$_4$, the PL intensity of SA-CN-1.0 sample is greatly suppressed, indicating the electron localization on the surface terminal sites [9]. The results suggested that acid modification was helpful to inhibit the recombination of photo-induced electron-hole pairs and effectively improve their separation efficiency [33].

3.2. Photocatalytic activity of acid-modified g-C$_3$N$_4$

The selective aerobic oxidation of benzyl alcohol to benzaldehyde under visible light irradiation is chosen as the assessment of photocatalytic activity of SA-CN samples. The results are shown in Table 2 . The product of oxidation of benzyl alcohol was primarily benzaldehyde. The mass balance of benzaldehyde and benzyl alcohol was >99% and no byproducts were detected. The controlled experiments are conducted in the cases of without light (entry 1) or no catalysts under visible light (entry 2) for 4 h. The results illustrate that the benzyl alcohol is difficult to be oxidized in the absence of light or catalysts. Under the same reaction condition, pure g-C$_3$N$_4$ showed low activity for the oxidation of benzyl alcohol, and the conversion of benzyl alcohol is only about 6.6% with 99% benzaldehyde selectivity under visible light irradiation for 4 h (entry 3). In contrast to the pure g-C$_3$N$_4$, significant

improvement of benzaldehyde yield could be achieved by modification of sulfuric acid. It was found that the activity of the acid-modified samples was greatly influenced by the concentrations of sulfuric acid. At the sulfuric acid concentration of 0.5 M, the conversion of benzyl alcohol is as high as 10.7% (entry 4). When the concentration increases to 1 M, the conversion of benzyl alcohol increases to 23.4%, which is over 2.5 times higher than that of the CN sample, while the selectivity to benzaldehyde is still higher than 98% (entry 5). However, higher concentration of sulfuric acid leads to decrease of conversion of benzyl alcohol (entry 6, 7). The present results indicated that a suitable sulfuric acid concentration is crucial for optimizing the photocatalytic activity of SA-CN materials. In the range of 1 M-3 M, although sulfuric acid treatment induced an obvious increase in surface area, the sample still exhibited decreased activity with increase of the sulfuric acid concentration. The results show that the excessive sulfuric acid modification is unfavorable for photocatalytic activity.

The activity of the acid-modified samples was also greatly influenced by reflux time of sulfuric acid treatment. The results are shown in entries 8–13 of Table 2. When the carbon nitride was refluxed by sulfuric acid (1 M) for 6 h, the photocatalytic activity is enhanced with 8.9% conversion and 99% benzaldehyde selectivity. When the reflux time is increased to 24 h, the conversion of alcohols increases gradually and the optimal photocatalytic performance is obtained. Further increase of the reflux time above 24 h leads to a decrease of photocatalytic activity. Clearly, the higher sulfuric acid concentration and longer treatment time would deactivate carbon nitride. It is inferred that excessive sulfuric acid treatment degrades the surface structure of carbon nitride that is responsible for the low catalytic activity.

Other inorganic and organic acids were also selected to investigate the effect of protonation on the photocatalytic activity (Table 3). It was observed that the activity of carbon nitride could be improved by the treatment of Brønsted or organic acids, and H$_2$SO$_4$ was found to be the most effective acid examined, indicating that surface acidity of carbon nitride is an important factor influencing its photocatalytic performance. It is known that β-hydride elimination to form an alkoxy intermediate is the rate-limiting step for the catalytic oxidation of alcohols [49]. In the photocatalytic oxidation system, the rate of photoredox-induced β-hydride elimination was mostly dependent on the charge separation efficiency at the interface. The presence of surface acidity on the catalysts surface would facilitate both the trapping of electrons by transferring of proton-coupled electron to oxygen and fast electron donation from the alcohol to the hole. Therefore, the β-hydride elimination in the photocatalysis system could be accelerated by acid modification.

Table 3
Photocatalytic performances of acid-modified g-C$_3$N$_4$ catalysts for oxidation of benzyl alcohol under visible light ($\lambda > 420$ nm).

Entry	Catalysts	hv	Conversion (%)	Benzaldehyde selectivity (%)
1	g-C$_3$N$_4$	+	6.6	>99
2	SA-CN-1.0	+	23.4	98
3	PhA–CN	+	16.5	99
4	HA–CN	+	20.2	99
5	FA–CN	+	12.8	99
6	AA–CN	+	10.8	>99
7	BA–CN	+	17.7	>99
8	PeA–CN	+	12.6	>99
9	NA–CN	+	16.9	99

Reaction performed at 100 °C for 4 h using trifluorotoluene as the solvent, 1 mmol benzyl alcohol, 50 mg catalyst.
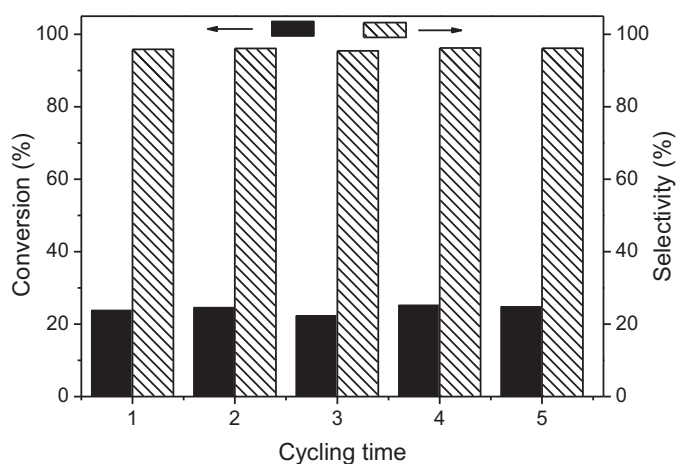
Fig. 10. stability test of SA-CN-1.0 sample for the selective oxidation of benzyl alcohol.

3.3. Stability test

In order to determine the stability of SA-CN photocatalyst, five times repeated experiments were carried out under the same conditions and the results were shown in Fig. 10 . SA-CN catalyst is able to maintain a stable and efficient activity to the selective aerobic oxidation of benzyl alcohol generally. Except for around a

Fig. 11. Results of mechanism experiments for bulk g-C₃N₄ (a) and SA-CN (b).

2% drop of conversion rate during the third run, there is no further deactivation for the sample in the long run. The structures of SA-CN-1.0 catalysts before and after reactions are also characterized by XRD and FTIR techniques (Fig. S1), which demonstrates that there is no measurable change in surfaces and structures after reactions. This also provides a premise for the catalyst in the practical applications.

3.4. Mechanism of photoactivity

To reveal the photocatalytic mechanism, the main oxidative species in the photocatalytic process were detected. In this photocatalytic reaction system, many active species might be involved, such as superoxide radicals ($\bullet O_2^-$), photogenerated holes, the hydroxyl radicals. So radical scavengers were adopted to sacrifice the above oxidative species to determine prominent active species. The results are shown in Fig. 11. For pure g-C₃N₄ photocatalytic system, the addition of *tert*-butyl alcohol has a little effect on conversion of benzyl alcohol, indicating hydroxyl radicals were not formed in the oxidation process. It is reasonable that the valence band potential of g-C₃N₄ is too low to directly oxidize hydroxyl group to form hydroxyl radicals in thermodynamics. When ammonium oxalate was added, the activity was decreased slightly. However, the activity declined dramatically by the addition of benzoquinone to the reaction solution. The above results indicate that holes are the minor active species, while ($\bullet O_2^-$) radicals are the main active species that is responsible for the oxidation of benzyl alcohol under visible light irradiation. When O₂ was replaced by N₂ in the photocatalytic system, the activity also declined significantly. As molecular O₂ is the important source for the generation of ($\bullet O_2^-$), the result provides evidence that ($\bullet O_2^-$) is the main active species. Similar to g-C₃N₄ photocatalytic system, both ($\bullet O_2^-$) radical and holes are responsible for the photocatalytic activity of SA-CN catalyst. ($\bullet O_2^-$)radical is still the main active species in the SA-CN photocatalytic system as the activity decreased obviously in the presence of benzoquinone.

Combined with experimental results including physicochemical and photocatalytic properties, it is inferred that the enhanced photocatalytic performance of SA-CN over the CN can be attributed to main reasons as follows: (1) the surface area of carbon nitride is improved greatly by sulfuric acid treatment, and the larger surface area can oers more adsorption sites and photocatalytic reaction centers; (2) the smaller structural size and nanoporous structure of SA-CN formed by the acid treatment makes the mass transfer easier in the reaction. Moreover, the porous structures are also beneficial to enhance photoadsorption efficiency. The presence of smaller structural size and porous structure are another reasons that account for the improved activity; (3) the enlarged band gap of SA-CN leads to a strengthened redox ability, also contributing to the enhanced photocatalytic activity; (4) the new acid sites on the surface of carbon nitride formed by acid treatment can promote β-hydride elimination in the photocatalytic oxidation of alcohols, which can be also considered as an important factor in the enhancement of the photocatalytic activity.

4. Conclusions

In summary, we have demonstrated the novel acid-modified g-C₃N₄ works as efficient catalysts in the selective aerobic oxidation of benzyl alcohol under visible light irradiation. Acid-modified g-C₃N₄ catalyst was synthesized by a facile method through reflux in different acidic substances. Under visible light irradiation, acid-modified g-C₃N₄ catalyst exhibited higher photocatalytic performance in the oxidation of benzyl alcohol to benzaldehyde in neutral condition than pure g-C₃N₄. Among acids examined, sulfuric acid-modified g-C₃N₄ displayed the best catalytic activity,
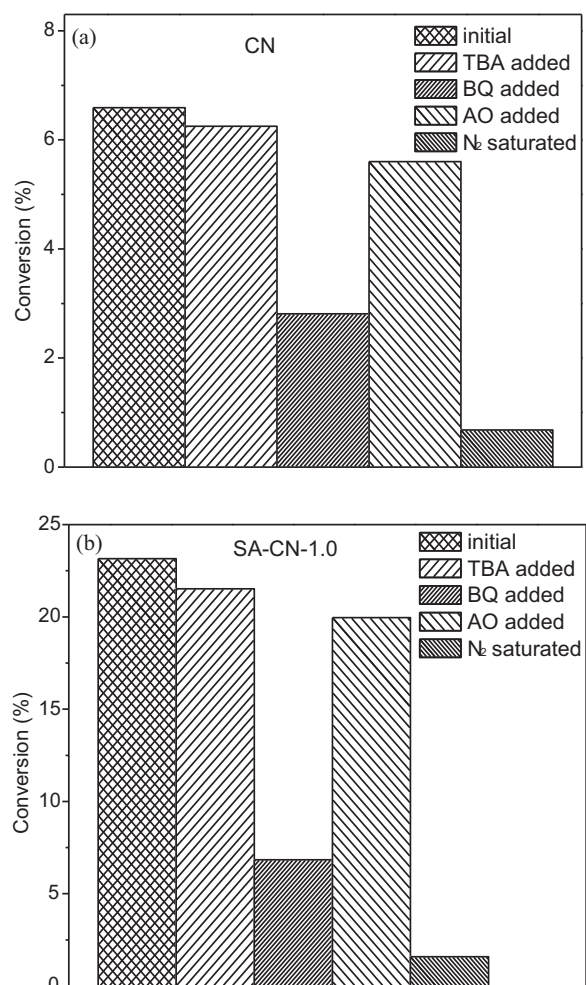
which was about 2.5 times higher than that of pure g-C$_3$N$_4$. The catalyst can be recyclable for five times without obvious deactivation. The enhanced catalytic performance has been attributed to the larger specific surface area, smaller structural size, larger band gap, enhanced surface chemical property by acid modification. Acid activation provides a facile and efficient way for g-C$_3$N$_4$ to enhance photocatalytic activity in the selective aerobic oxidation of benzyl alcohol, which makes it a promising candidate for a large scale of potential applications in selective organic transformation.

Acknowledgements

Appendix A. Supplementary data

Supplementary data associated with this article can be found, in the online version, at http://dx.doi.org/10.1016/j.materresbull.2014.06.021.

References

[1] D. Lenoir, Selective oxidation of organic compounds-sustainable catalytic reactions with oxygen and without transition metals? Angew. Chem. Int. Ed. 45 (2006) 3206–3210.

[2] G.W. Zhan, Y.L. Hong, V.T. Mbah, J.L. Huang, A.R. Ibrahim, M.M. Du, Q.B. Li, Bimetallic Au-Pd/MgO as efficient catalysts for aerobic oxidation of benzyl alcohol: A green bio-reducing preparation method, Appl. Catal. A: Gen. 439 (2012) 179–186.

[3] Y. Su, L.C. Wang, Y.M. Liu, Y. Cao, H.Y. He, K.N. Fan, Microwave-accelerated solvent-free aerobic oxidation of benzyl alcohol over efficient and reusable manganese oxides, Catal. Commun. 8 (2007) 2181–2185.

[4] Y.M. Liu, H. Tsunoyama, T. Akita, T. Tsukuda, Preparation of ∼1 nm gold clusters confined within mesoporous silica and microwave-assisted catalytic application for alcohol oxidation, J. Phys. Chem. C 113 (2009) 13457–13461.

[5] Y. Leng, J. Wang, P.P. Jiang, Amino-containing cross-linked ionic copolymer-anchored heteropoly acid for solvent-free oxidation of benzyl alcohol with H$_2$O$_2$, Catal. Commun. 27 (2012) 101–104.

[6] S. Mayavan, H.S. Jang, M.J. Lee, S.H. Choi, S.M. Choi, Enhancing the catalytic activity of Pt nanoparticles using poly sodium styrene sulfonate stabilized graphene supports for methanol oxidation, J. Mater. Chem. A 1 (2013) 3489–3494.

[7] H. Chen, Q.H. Tang, Y.T. Chen, Y.B. Yan, C.M. Zhou, Z. Guo, X.L. Jia, Y.H. Yang, Microwave-assisted synthesis of PtRu/CNT and PtSn/CNT catalysts and their applications in the aerobic oxidation of benzyl alcohol in base-free aqueous solutions, Catal. Sci. Technol. 3 (2013) 328–338.

[8] P.F. Zhang, Y. Wang, J. Yao, C.M. Wang, C. Yan, M. Antonietti, H.R. Li, Visible-light-induced metal-free allylic oxidation utilizing a coupled photocatalytic system of g-C$_3$N$_4$ and N-hydroxy compounds, Adv. Synth. Catal. 353 (2011) 1447–1451.

[9] X.C. Wang, K. Maeda, X.F. Chen, K. Takanabe, K. Domen, Y.D. Hou, X.Z. Fu, M. Antonietti, Polymer semiconductors for artificial photosynthesis: hydrogen evolution by mesoporous graphitic carbon nitride with visible light, J. Am. Chem. Soc. 131 (2009) 1680–1681.

[10] P.F. Zhang, Y. Wang, H.R. Li, M. Antonietti, Metal-free oxidation of sulfides by carbon nitride with visible light illumination at room temperature, Green Chem. 14 (2012) 1904–1908.

[11] Y.H. Zhang, Y.J. Xu, Bi$_2$WO$_6$: a highly chemoselective visible light photocatalyst toward aerobic oxidation of benzylic alcohols in water, RSC Adv. 4 (2014) 2904–2910.

[12] L. Ge, C.C. Han, J. Liu, Novel visible light-induced g-C$_3$N$_4$/Bi$_2$WO$_6$ composite photocatalysts for efficient degradation of methyl orange, Appl. Catal. B: Environ. 108-109 (2011) 100–107.

[13] X.M. Wang, G.J. Wu, N.J. Guan, L.D. Li, Supported Pd catalysts for solvent-free benzyl alcohol selective oxidation: effects of calcination pretreatments and reconstruction of Pd sites, Appl. Catal. B: Environ. 115 (2012) 7–15.

[14] S. Obregon, G. Colon, Improved H$_2$ production of Pt-TiO$_2$/g-C$_3$N$_4$-MnO$_x$ composites by an efficient handling of photogenerated charge pairs, Appl. Catal. B: Environ. 144 (2014) 775–782.

[15] C.J. Li, G.R.B. Xua h. Zhang, J.R. Gong, High selectivity in visible-light-driven partial photocatalytic oxidation of benzyl alcohol into benzaldehyde over single-crystalline rutile TiO$_2$ nanorods, Appl. Catal. B: Environ. 115-116 (2012) 201–208.

[16] L. Özcana, S. Yurdakal, V. Augugliaro, V. Loddo, S. Palmas, G. Palmisano, L. Palmisano, Photoelectrocatalytic selective oxidation of 4-methoxybenzyl alcohol in water by TiO$_2$ supported on titanium anodes, Appl. Catal. B: Environ. 132-133 (2013) 535–542.

[17] N. Zhang, Y.H. Zhang, X.Y. Pan, M.Q. Yang, Y.J. Xu, Constructing ternary CdS-graphene-TiO$_2$ hybrids on the flatland of graphene oxide with enhanced visible-light photoactivity for selective transformation, J. Phys. Chem. C 116 (2012) 18023–18031.

[18] D. Spasianoa, L.D.P. Rodriguez, J.C. Olleros, S. Malato, R. Marotta, R. Andreozzi, TiO$_2$/Cu(II) photocatalytic production of benzaldehyde from benzyl alcohol in solar pilot plant reactor, Appl. Catal. B: Environ. 136–137 (2013) 56–63.

[19] L.J. Shen, L.J. Liang, W.M. Wu, R.W. Liang, L. Wu, CdS-decorated UiO-66(NH$_2$) nanocomposites fabricated by a facile photodeposition process: an efficient and stable visible-light-driven photocatalyst for selective oxidation of alcohols, J. Mater. Chem. A 1 (2013) 11473–11482.

[20] N. Zhang, M.Q. Yang, Z.R. Tang, Y.J. Xu, CdS-graphene nanocomposites as visible light photocatalyst for redox reactions in water: a green route for selective transformation and environmental remediation, J. Catal. 303 (2013) 60–69.

[21] N. Zhang, S.Q.X.Z. Liu Fu, Y.J. Xu, Fabrication of coenocytic Pd@CdS nanocomposite as a visible light photocatalyst for selective transformation under mild conditions, J. Mater. Chem. 22 (2012) 5042–5052.

[22] Y.H. Zhang, N. Zhang, Z.R. Tang, Y.J. Xu, Transforming CdS into an efficient visible light photocatalyst for selective oxidation of saturated primary C–H bonds under ambient conditions, Chem. Sci. 3 (2012) 2812–2822.

[23] S.Q.M.Q. Liu Yang, Y.J. Xu, Surface charge promotes the synthesis of large, flat structured graphene-(CdS nanowire)-TiO$_2$ nanocomposites as versatile visible light photocatalysts, J. Mater. Chem. A 2 (2014) 430–440.

[24] C. Giordano, M. Antonietti, Synthesis of crystalline metal nitride and metal carbide nanostructures by sol–gel chemistry, Nano Today 6 (2011) 366–380.

[25] F.Z. Su, S.C. Mathew, G. Lipner, X.Z. Fu, M. Antonietti, S. Blechert, X.C. Wang, mpg-C$_3$N$_4$-catalyzed selective oxidation of alcohols using O$_2$ and visible light, J. Am. Chem. Soc. 132 (2010) 16299–16301.

[26] X.F. Chen, J.S. Zhang, X.Z. Fu, M. Antonietti, X.C. Wang, Fe-g-C$_3$N$_4$-catalyzed oxidation of benzene to phenol using hydrogen peroxide and visible light, J. Am. Chem. Soc. 131 (2009) 11658–11659.

[27] Y. Wang, X.C. Wang, M. Antonietti, Polymeric graphitic carbon nitride as a heterogeneous organocatalyst: from photochemistry to multipurpose catalysis to sustainable chemistry, Angew. Chem. Int. Ed. 51 (2012) 68–89.

[28] S.W.J.G. Cao Yu, g-C$_3$N$_4$ based photocatalysts for hydrogen production, J. Phys. Chem. Lett. 5 (2014) 2101–2107.

[29] T. Sano, S. Tsutsui, K. Koike, T. Hirakawa, Y. Teramoto, N. Negishi, K. Takeuchi, Activation of graphitic carbon nitride (g-C$_3$N$_4$) by alkaline hydrothermal treatment for photocatalytic NO oxidation in gas phase, J. Mater. Chem. A 1 (2013) 6489–6496.

[30] P.F. Zhang, H.R. Li, Y. Wang, Post-functionalization of graphitic carbon nitrides by grafting organic molecules: toward C–H bond oxidation using atmospheric oxygen, Chem. Commun. 50 (2014) 6312–6315.

[31] J.S. Zhang, X.F. Chen, K. Takanabe, K. Maeda, K. Domen, J.D. Epping, X.Z. Fu, M. Antonietti, X.C. Wang, Synthesis of a carbon nitride structure for visible-light catalysis by copolymerization, Angew. Chem. Int. Ed. 49 (2010) 441–444.

[32] X.C. Wang, K. Maeda, A. Thomas, K. Takanabe, G.J.M. Xin Carlsson, K. Domen, M. Antonietti, A metal-free polymeric photocatalyst for hydrogen production from water under visible light, Nat. Mater. 8 (2009) 76–80.

[33] L.G. Zhang, X.F. Chen, J. Guan, Y.J. Jiang, T.G.X.D. Hou Mu, Facile synthesis of phosphorus doped graphitic carbon nitride polymers with enhanced visible-light photocatalytic activity, Mater. Res. Bull. 48 (2013) 3485–3491.

[34] Y.J. Zhang, T. Mori, J.H. Ye, Polymeric carbon nitrides: semiconducting properties and emerging applications in photocatalysis and photoelectro-chemical energy conversion, Sci. Adv. Mater. 4 (2012) 282–291.

[35] Y.J. Zhang, A. Thomas, M. Antonietti, X.C. Wang, Activation of carbon nitride solids by protonation: morphology changes, enhanced ionic conductivity, and photoconduction experiments, J. Am. Chem. Soc. 131 (2009) 50–51.

[36] N. Kovtyukhova, Y.X. Wang, R.T. Lv, M. Terrones, V. Crespi, T. Mallouk, Reversible intercalation of hexagonal boron nitride with bronsted acids, J. Am. Chem. Soc. 135 (2013) 8372–8381.

[37] J.F. Huang, H.C.D. Luo Liang, I.W.G.A. Sun Baker, S. Dai, Hydrophobic bronsted acid-base ionic liquids based on PAMAM dendrimers with high proton conductivity and blue photoluminescence, J. Am. Chem. Soc. 127 (2005) 12784–12785.

[38] B.H. Long, Z.X. Ding, X.C. Wang, Carbon nitride for the selective oxidation of aromatic alcohols in water under visible light, ChemSusChem 6 (2013) 2074–2078.

[39] X.C. Wang, X.F. Chen, A. Thomas, X.Z. Fu, M. Antonietti, Metal-containing carbon nitride compounds: a new functional organic-metal hybrid material, Adv. Mater. 21 (2009) 1609–1612.

[40] X.B.J.T. Yan Chen, Q.J.P. Xue Miele, Synthesis and magnetic properties of CoFe$_2$O$_4$ nanoparticles confined within mesoporous silica, Micropor. Mesopor. Mater. 135 (2010) 137–142.

[41] A. Thomas, A. Fischer, F. Goettmann, M. Antonietti, J.O. Müller, R. Schlögl, J.M. Carlsson, Graphitic carbon nitride materials: variation of structure and morphology and their use as metal-free catalysts, J. Mater. Chem. 18 (2008) 4893–4908.

[42] S.B. Yang, Y.J. Gong, J.S. Zhang, L. Zhan, L.L. Ma, Z.Y. Fang, R. Vajtai, X.C. Wang, P. M. Ajayan, Exfoliated graphitic carbon nitride nanosheets as efficient catalysts for hydrogen evolution under visible light, Adv. Mater. 25 (2013) 2452–2456.

[43] J.D. Hong, X.Y.Y.S. Xia Wang, R. Xu, Mesoporous carbon nitride with in situ sulfur doping for enhanced photocatalytic hydrogen evolution from water under visible light, J. Mater. Chem. 22 (2012) 15006–15012.

[44] Y. Wang, J.S. Zhang, X.C. Wang, M. Antonietti, H.R. Li, Boron-and fluorine-containing mesoporous carbon nitride polymers: metal-free catalysts for cyclohexane oxidation, Angew. Chem. Int. Ed. 49 (2010) 3356–3359.

[45] Y.Z. Su, Y. Zhang, X.D. Zhuang, S. Li, D.Q. Wu, F. Zhang, X.L. Feng, Low-temperature synthesis of nitrogen/sulfur co-doped three-dimensional gra-phene frame works as efficient metal-free electrocatalyst for oxygen reduction reaction, Carbon 62 (2013) 296–301.

[46] Z.X. Ding, X.F. Chen, M. Antonietti, X.C. Wang, Synthesis of transition metal-modified carbon nitride polymers for selective hydrocarbon oxidation, ChemSusChem 4 (2011) 274–281.

[47] M. Okamura, A. Takagaki, M. Toda, J.N. Kondo, K. Domen, T. Tatsumi, M. Hara, S. Hayashi, Acid-catalyzed reactions on flexible polycyclic aromatic carbon in amorphous carbon, Chem. Mater. 18 (2006) 3039–3045.

[48] X.D. Zhang, X.H. Xie Wang, J.J. Zhang, B.C.Y. Pan Xie, Enhanced photoresponsive ultrathin graphitic-phase C_3N_4 nanosheets for bioimaging, J. Am. Chem. Soc. 135 (2013) 18–21.

[49] J.A. Mueller, C.P. Goller, M.S. Sigman, Elucidating the significance of beta-hydride elimination and the dynamic role of acid/base chemistry in a palladium-catalyzed aerobic oxidation of alcohols, J. Am. Chem. Soc. 126 (2004) 9724–9734.